# A Dynamic Hysteresis Prediction Model of Ultra-Thin GO Silicon Steel Under Multi-Harmonic Excitation

Haoming Wang , *Member, IEEE*, Xuanyuan Zhang, Xiaojun Zhao , *Member, IEEE*, Shengze Gao , *Graduate Student Member, IEEE*, Xinyi Wu, Yan Zhang , and Yu Miao

*Abstract*—The main work of this paper is to propose a dynamic hysteresis model to predict magnetic hysteresis characteristics for ultra-thin grain-oriented (GO) silicon steel under multi-harmonic excitation. First, the non-linear magnetization property of silicon steel is taken into consideration. Based on segmentation linear approximation, a new expression of eddy current field is obtained regarding unsaturated and saturated magnetization state, and the expression of excess field is improved by segmented statistical parameter $V_0$. Furthermore, a dynamic model for predicting hysteresis characteristics under multi-harmonic excitation is proposed. Simulated and predicted results are compared with the measured one, and the accuracy of the proposed model is verified.

*Index Terms*—Magnetic hysteresis, magnetic losses, power system harmonics, soft magnetic materials.

## I. INTRODUCTION

ULTRA-THIN GO silicon steel is always employed as the core in medium-frequency power transformers due to its exceptional soft magnetic properties [1]. Accurate prediction of the loss and hysteresis characteristics of the core is vital for the overall design of the unit [2]. Due to the increasingly high operating frequency and the wide application of power electronics, the dynamic loss and hysteresis characteristics of ultra-thin GO silicon steel will be influenced by skin effect and harmonics. Minor loops and asymmetrical loops will be formed under the influence of harmonics. Hence, it is important to propose a dynamic hysteresis model that can accurately predict dynamic hysteresis characteristics under high-frequency and multi-harmonic excitations.

Steinmetz's equation is a widely used empirical equation for loss calculation. But its accuracy under multi-harmonic excitation requires complex parameter identification, and it fails to simulate the hysteresis characteristics. The loss separation method divides the whole loss into hysteresis loss, eddy current loss, and excess loss, providing field expressions for each component of the loss [3]. But the original method can only be applied to sinusoidal excitation. To broaden applicability of the loss separation method, a model is proposed to predict inner symmetrical minor loops by introducing loss coefficient in the original energetic model [4]. However, this model cannot consider the asymmetrical minor loops and requires extraction of numerous parameters. A method considering DC-bias is proposed in [5]. But the expression of eddy-current field and the statistical parameter of excess is lack of consideration of skin effect, limiting its applicability to low-frequency excitations. Subsequently, a method considering skin effect is proposed in [6]. However, it lacks a clear physical meaning in the derivation of the eddy current field and the accuracy of the modeled loops depends on shape factors and it may not work well with multi-harmonic excitations. In summary, the previous methods lack clear physically meaningful derivation of the expression of eddy current field that takes skin effect into consideration, and cannot accurately predict the dynamic hysteresis loops under complex harmonic excitations.

In this paper, the eddy current field corresponding to various magnetization states is obtained by establishing a linear segmental approximation to the non-linear *B-H* relationship. And the segmented statistical parameter $V_0$ is utilized to establish a relationship between excess field and different magnetization states. A new parameter identification approach is introduced for the eddy current field. A dynamic hysteresis model for multi-harmonic excitation is derived, and its accuracy is confirmed through a comparison with measured hysteresis loops.

Haoming Wang, Xuanyuan Zhang, Xiaojun Zhao, Shengze Gao, and Xinyi Wu are with the Department of Electrical Engineering, North China Electric Power University, Baoding 071003, China (e-mail: hmwang@ncepu.edu.cn; zxyncepu@ncepu.edu.cn; zxjncepu@ncepu.edu.cn; 120222101012@ncepu.edu.cn; wxy990913@163.com).

Yan Zhang is with the Ningbo Institute of Materials Technology and Engineering, Chinese Academy of Science, Ningbo 315201, China (e-mail: yzhang@nimte.ac.cn).

Yu Miao is with the Electric Power Research Institute of Guizhou Power Grid Company, Ltd., Guiyang 550002, China (e-mail: 574122104@qq.com).

## II. MEASUREMENT OF MAGNETIC PROPERTIES

A magnetic property testing platform is configured [5]. The type of ultra-thin GO silicon steel is 15SQF1300, and the dimension for the tested sample is 600 mm 100 mm × 0.1458 mm. Note that, the quasi-static hysteresis loops are approximated by
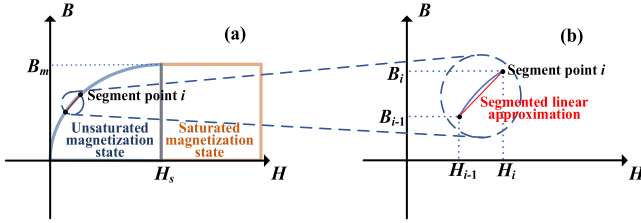
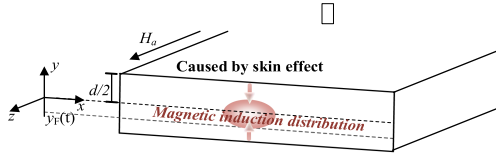Fig. 1.    Segmented $B$-$H$ relationship in unsaturated state.



Fig. 2.    Schematic diagram of soft magnetic materials.

the hysteresis loops measured at 5 Hz since the DC excitation is difficult to be achieved due to the limitation of equipment.

## III. DYNAMIC HYSTERESIS MODEL UNDER SINGLE FREQUENCY SINUSOIDAL EXCITATION

Based on the loss separation model proposed by Bertotti, the dynamic field $H_t$ can be expressed as (1).

$$H_t = H_{hy} + H_{cl} + H_{ex} \qquad (1)$$

where $H_{hy}$, $H_{cl}$ and $H_{ex}$ are the magnetic field corresponding to hysteresis filed, eddy current field and excess field respectively.

### A. Dynamic Part of Field

As depicted in Fig. 1(a), the magnetization curve exhibits two distinct parts, namely the unsaturated magnetization state and the saturated magnetization state. To facilitate analysis, the unsaturated magnetization part will be approximated by segmented linearity, as illustrated in Fig. 1(b). The $H_s$ is saturated magnetic field strength, and $B_m$ is the corresponding magnetic induction. For each division point i, the $H_i$ and $B_i$ are the corresponding magnetic field strength and magnetic induction. For each segment, the $B$-$H$ relationship is approximated by $B = \mu_i H + B_{0,i}$. The $\mu_i$ and $B_{0,i}$ refer to magnetic permeability corresponding to point i, respectively.

Fig. 2 illustrates a schematic diagram of soft magnetic materials. When the applied field $H_a$ is oriented parallel to the z-axis, the internal magnetic induction distribution only varies along the y-axis direction. Based on these assumptions, the Maxwell's equations of each segment are shown in (2).

$$\frac{\partial^2 H_i(y,t)}{\partial y^2} = \sigma \mu_i \frac{\partial H_i(y,t)}{\partial t} \qquad (2)$$

where $\omega = 2\pi f$, $f$ represents frequency.

Note that, all field strength mentioned in the following text, refers to the average field strength. Applying a sinusoidal excitation, $H_{a,i} = H_{m,i}\exp(-j\omega t)$, by solving (2), the internal magnetic induction distribution can be obtained as (3).

$$H_i(t) = \varsigma H_{m,i} \frac{\sqrt{2}\delta_{d,i}}{d} e^{-j(\omega t - \tau_i)} \qquad (3)$$

$$\varsigma = \sqrt{\frac{ch(d/\delta_{d,i}) - \cos(d/\delta_{d,i})}{ch(d/\delta_{d,i}) + \cos(d/\delta_{d,i})}} \qquad (4)$$

$$\tan(\tau_i) = \frac{sh(d/\delta_{d,i}) - \sin(d/\delta_{d,i})}{sh(d/\delta_{d,i}) + \sin(d/\delta_{d,i})} \qquad (5)$$

where $\delta_{d,i}$ represents skin depth, taking $1/(f\pi\sigma\mu_i)^{0.5}$, $\sigma$ designates the conductivity.

While the peak induction $B_{m,i}$ is given, the relationship between $H_{m,i}$ and $B_{m,i}$ can be expressed as (6).

$$H_{m,i} = \varsigma \frac{dB_{m,i}}{\sqrt{2}\mu_i\delta_{d,i}} \qquad (6)$$

Then by subtracting the internal field strength from the applied field strength, the eddy current field strength can be derived as shown in (7).

$$H_{cl,i}(t) = \text{Re}[H_{a,i}(t) - H_i(t)]$$
$$= H_{m,i}\sqrt{(g(\delta_{d,i}) - \cos(\psi_i))^2 + \sin^2(\psi_i)} \cos(\omega t + \theta_i - \tau_i) \qquad (7)$$

$$\begin{cases} g(\delta_{d,i}) = \frac{\delta_{d,i}}{d}\sqrt{2 \cdot \frac{ch(d/\delta_{d,i}) - \cos(d/\delta_{d,i})}{ch(d/\delta_{d,i}) + \cos(d/\delta_{d,i})}} \\ \tan(\theta_i) = \frac{g(\delta_{d,i})\sin(\tau_i)}{g(\delta_{d,i})\cos(\tau_i) - 1} \end{cases} \qquad (8)$$

Given the high value of $B_m$, the saturation magnetization state shown in Fig. 1(a) should be taken into consideration. Therefore, it is necessary to segment it into saturated magnetization regions and unsaturated magnetization regions, and utilize parameter $y_F$ to ascertain the boundary between the two regions, as shown in Fig. 2.

$$y_F(t) = \begin{cases} \frac{d}{4}\left(\frac{B(t)}{B_m} - 1\right), & \frac{dB}{dt} > 0 \\ -\frac{d}{4}\left(\frac{B(t)}{B_m} + 1\right), & \frac{dB}{dt} < 0 \end{cases} \qquad (9)$$

By solving Maxwell's equations, the internal magnetic field distribution while $dB/dt>0$ can be obtained as

$$H(y,t) =$$
$$\begin{cases} \frac{\pi f\sigma dB_m}{4} \cdot e^{-j\omega\left(t+\frac{\pi}{2}\right)} \cdot \left(e^{-j\omega t} - 1 - \frac{4y}{d}\right), & \frac{d}{2} \leq y < y_F(t) \\ H_{m,i}\frac{\cos[(1+j)y/\delta_{d,i}]}{\cos[(1+j)d/2\delta_{d,i}]}e^{-j\omega t}, & y_F(t) < y \leq 0 \end{cases} \qquad (10)$$

The magnetic field distribution while $dB/dt<0$ can be obtained similarly. The applied filed strength $H_a(t)$ can be obtained by taking $y = d/2$ in (10). Then the eddy-current field for saturated magnetization state can be derived as (11).

$$H_{cl}(t) = \text{Re}[H_a(t) - H(t)]$$
$$\frac{\omega\sigma d^2 B_m}{32}\sin(\omega t)[-\delta \cdot 4\cos(\omega t) - 3 + e^{-(\omega t)^2}]$$
$$- \frac{H_{m,i}}{4}(\delta \cdot \cos(\omega t) - 1)\cdot$$
$$H_{m,i}\sqrt{(g(\delta_{d,i}) - \cos(\psi_i))^2 + \sin^2(\psi_i)}\cos(\omega t + \theta_i - \tau_i) \qquad (11)$$
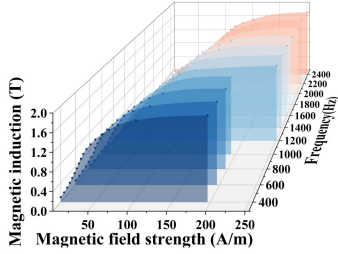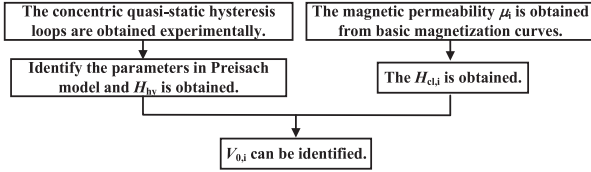
Fig. 3.    Basic magnetization curves.



Fig. 4.    Flow chart of parameters identification.

where $\delta = \pm 1$ and depends on if the magnetic induction is increasing or decreasing.

Eddy current loss is characterized by the superposition of eddy current effects generated at different magnetic domain walls, and excess loss is directly proportional to average loss [3]. It is necessary to segment excess losses based on varying magnetic permeability values [6], as shown in (12).

$$H_{ex,i} = \sqrt{\sigma S V_{0,i} G} \cdot \delta \cdot \left| \frac{dB(t)}{dt} \right|^{0.5} \qquad (12)$$

where $S$ is the cross-sectional area of specimen. $G$ is the dimensionless parameter, taking 0.1356. $V_{o,i}$ is the statical parameter that needs to be identified for segment i.

Then the eddy current field $H_{cl,i}$ and excess field $H_{ex,i}$ corresponding to each segment can be determined. Therefore, the dynamic part of field expression $H_{dy,i}$ can be obtained as,

$$H_{dy,i} = H_{cl,i} + H_{ex,i} \qquad (13)$$

By concatenating the dynamic part of fields of each segment $H_{dy,i}$, the total dynamic field $H_{dy}$ can be obtained. Then the total loss $W_t$ can be obtained as (14).

$$W_t = \oint_C (H_{hy} + H_{dy})dB \qquad (14)$$

### B. Identification of Parameters

The skin depth $\delta_{d,i}$ of each segment and associated parameters are determined by the permeability $\mu_i$. As depicted in Fig. 3, the basic magnetization curves, varying with frequency, are obtained from concentric hysteresis loops, respectively. Then the $\mu_i$ can be determined. The number of segments is determined by the required simulation accuracy.

Utilizing the Preisach model and the previously mentioned parameter identification, it becomes feasible to determine the quasi-static field $H_{hy}$ and eddy-current field $H_{cl,i}$ of each segment. Then the statistical parameter $V_{0,i}$ in $H_{ex,i}$ for each segment can be determined. Fig. 4 presents a comprehensive flow chart depicting the identification process of all parameters.
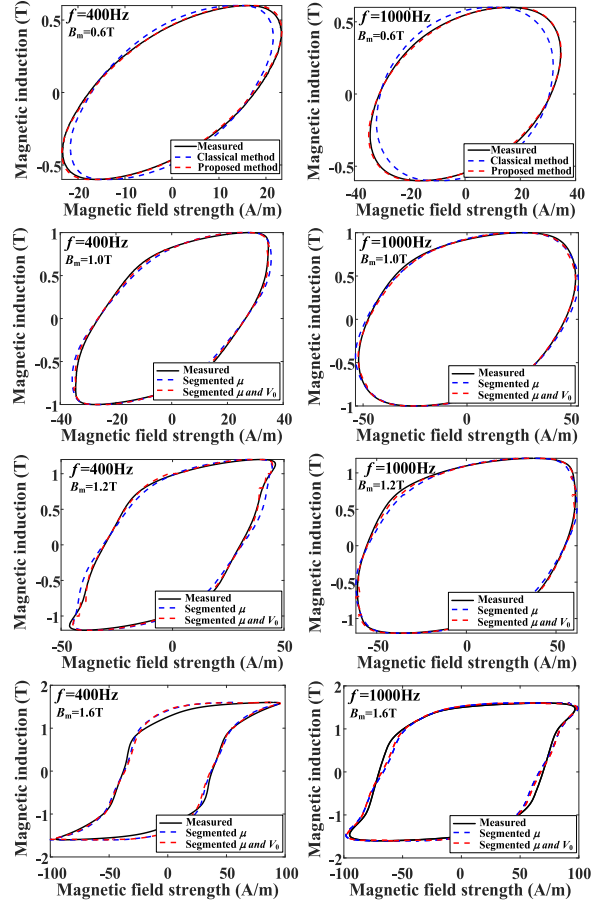


Fig. 5.    Comparison between the simulated and measured results under single frequency excitations.

TABLE I
SIMULATION DEVIATION BY DIFFERENT MODELS

| MAD/error(%) | | | Segmented $\mu$ and $V_o$ | Segmented $\mu$ | Classical method |
|---|---|---|---|---|---|
| $f$ (Hz) | 400 | $B_m$ (T) 0.6 | 3.68/0.33 | 3.68/0.33 | 14.41/1.35 |
| | | 1.0 | 4.44/0.10 | 7.43/0.23 | 15.33/1.38 |
| | | 1.2 | 4.98/0.69 | 9.18/1.77 | 16.91/1.18 |
| | | 1.6 | 3.78/4.55 | 4.14/5.12 | 16.77/5.34 |
| | 1000 | $B_m$ (T) 0.6 | 2.85/0.10 | 2.85/0.10 | 19.59/1.33 |
| | | 1.0 | 3.96/0.67 | 5.57/1.05 | 19.34/1.43 |
| | | 1.2 | 3.85/0.29 | 6.25/1.42 | 16.36/1.577 |
| | | 1.6 | 7.2/0.22 | 9.26/0.43 | 13.29/1.43 |

### C. Results Under Single-Frequency Excitations

Fig. 5 depicts the comparative analysis between the simulated dynamic hysteresis loops and measured one.

To assess the fitting accuracy of hysteresis loops, the Mean Absolute Deviation (MAD) is introduced as (15). The results of loss deviation and MAD are shown in Table I.

$$MAD = \frac{1}{M} \sum_{i=1}^{M} \left| \frac{H_{i,cal} - H_{i,mea}}{H_{i,mea}} \right| \qquad (15)$$

where $M$ is the total number of data points.

TABLE II
PREDICTION DEVIATION

| | PREDICTION DEVIATION | | |
|---|---|---|---|
| Condition | $W_{mea}$(W/kg) | $W_{cal}$(W/kg) | error(%) |
| 1 | 11.21 | 11.53 | 2.84 |
| 2 | 14.97 | 15.67 | 4.69 |
| 3 | 12.74 | 13.03 | 2.25 |
| 4 | 18.16 | 18.35 | 1.07 |

As shown in Table I, the MAD of the proposed method is significantly lower than that of the classical method mentioned in [3], which indicates the high accuracy of the proposed method in fitting hysteresis loops. Additionally, it is evident that incorporating the segmented statistical parameter $V_0$, as opposed to relying solely on segmented permeability, can effectively enhance the fitting accuracy of hysteresis loops.

## IV. DYNAMIC HYSTERESIS MODEL UNDER MULTI-HARMONIC EXCITATION

The magnetic induction $B_{arb}(t)$ under multi-harmonic excitations can be expressed as,

$$\begin{cases} B_{arb}(t) = B_{m,1}\cos(\omega t) + \sum_{k=2}^{p} B_{m,k}\cos(k\omega t + \varphi_k) \\ \eta_k = B_{m,k}/B_{m,1} \end{cases}$$
(16)

where $B_{m,1}$, $B_{m,k}$ designate the amplitude of magnetic induction corresponding to fundamental harmonic and $k$th harmonic, respectively. $p$ is the total number of harmonics.

The regarding field strength $H_{arb}(B_{arb},t)$ can be expressed as,

$$H_{arb}(B_{arb}, t) = H_{hy,arb} + H_{cl,arb} + H_{ex,arb}$$
(17)

where $H_{hy,arb}, H_{cl,arb}, H_{ex,arb}$ represents quasi-static hysteresis field, eddy-current field and excess field respectively.

The expression of excess field is shown in (18).

$$H_{ex,arb}(t) = \sqrt{\sigma SG}\delta \cdot \left[\sum_{k=1}^{n} V_{0,k}(B_{m,k}, f_k, \mu_i) \cdot \left|\frac{dB_{arb,k}(t)}{dt}\right|\right]^{0.5}$$
(18)

where $B_{arb,k}$ denote the $k$th harmonics. $\mu_i$ is the segmented magnetic permeability corresponding to $k$th harmonic.

Since harmonic distortion in power systems is restricted to a small range, the formula for eddy currents under harmonic excitation can be derived as (19) by using (7),

$$H_{cl,arb}(t) = \sum_{k=1}^{p} H_{cl,k}(t)$$
(19)

where $H_{cl,k}$ is the eddy current field regarding to $k$th harmonics.

Four harmonic excitations with a fundamental frequency of 400 Hz are used to validate the accuracy. As shown in Fig. 6 and Table II, the maximum predicted loss error is 4.69%, validating the accuracy of the proposed model in terms of loss prediction under multi-harmonic excitations.
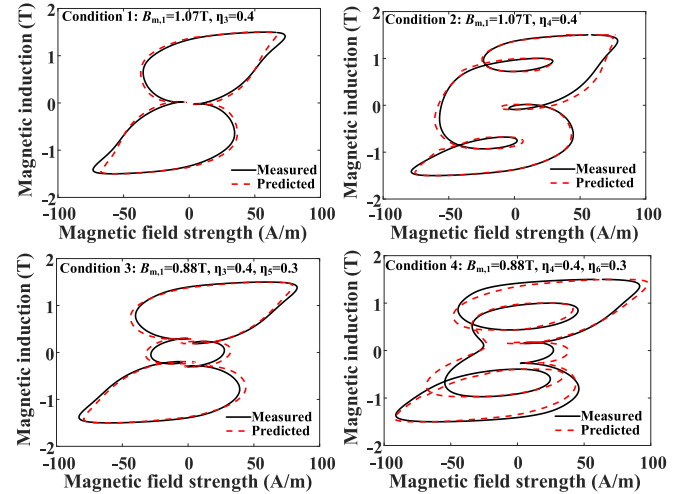


Fig. 6. Predicted and measured hysteresis loops under harmonic excitations.

## V. CONCLUSION

This study presents a dynamic hysteresis model for accurate hysteresis simulation under single-frequency excitation. However, as $B_m$ approaches saturation, the improvement in hysteresis loop fitting accuracy does not show significant enhancement with an increase in the number of segments or the segmentation extraction of $V_0$. With the identification of parameters under single-frequency excitation, accurate prediction of hysteresis characteristics under multi-harmonic excitation becomes feasible.

## REFERENCES

[1] T. Kauder, T. Belgrand, R. Lemaître, A. Thul, and K. Hameyer, "Medium-frequency power transformer using GOES for a three-phase dual active bridge," *J. Magnetism Magn. Mater.*, vol. 504, Jun. 2020, Art. no. 166672, doi: 10.1016/j.jmmm.2020.166672.

[2] H. Zhao, C. Ragusa, C. Appino, O. de la Barrière, Y. Wang, and F. Fiorillo, "Energy losses in soft magnetic materials under symmetric and asymmetric induction waveforms," *IEEE Trans. Power Electron.*, vol. 34, no. 3, pp. 2655–2665, Mar. 2019, doi: 10.1109/tpel.2018.2837657.

[3] G. Bertotti, "General properties of power losses in soft ferromagnetic materials," *IEEE Trans. Magn.*, vol. 24, no. 1, pp. 621–630, Jan. 1988, doi: 10.1109/20.43994.

[4] R. Liu and L. Li, "Accurate symmetrical minor loops calculation with a modified energetic hysteresis model," *IEEE Trans. Magn.*, vol. 56, no. 3, Mar. 2020, Art. no. 7510204, doi: 10.1109/tmag.2019.2956475.

[5] X. Zhao, H. Xu, Z. Cheng, Z. Du, L. Zhou, and D. Yuan, "A simulation method for dynamic hysteresis and loss characteristics of GO silicon steel sheet under non-sinusoidal excitation," *IEEE Trans. Appl. Supercond.*, vol. 31, no. 8, Nov. 2021, Art. no. 8200304, doi: 10.1109/tasc.2021.3091084.

[6] X. Zhao, L. Yang, H. Xu, K. Huang, L. Liu, and Z. Du, "Dynamic hysteresis and loss modelling of grain-oriented silicon steel under high-frequency sinusoidal excitation," *IEEE Trans. Magn.*, vol. 58, no. 9, Sep. 2022, Art. no. 7300805, doi: 10.1109/tmag.2022.3179912.

[7] S. E. Zirka, Y. I. Moroz, R. G. Harrison, and N. Chiesa, "Inverse hysteresis models for transient simulation," *IEEE Trans. Power Del.*, vol. 29, no. 2, pp. 552–559, Apr. 2014, doi: 10.1109/tpwrd.2013.2274530.